Photonic Floquet Skin-Topological Effect

Yeyang Sun,[1,*] Xiangrui Hou,[1,*] Tuo Wan,[1] Fangyu Wang,[1] Shiyao Zhu,[1,2] Zhichao Ruan,[1,2,†] and Zhaoju Yang[1,‡]

[1]*School of Physics and Zhejiang Province Key Laboratory of Quantum Technology and Device,*
Zhejiang University, Hangzhou 310027, Zhejiang Province, China
[2]*State Key Laboratory for Extreme Photonics and Instrumentation, Zhejiang University,*
Hangzhou 310027, China

Non-Hermitian skin effect and photonic topological edge states are of great interest in non-Hermitian physics and optics. However, the interplay between them is largely unexplored. Here, we propose and demonstrate experimentally the non-Hermitian skin effect constructed from the nonreciprocal flow of Floquet topological edge states, which can be dubbed "Floquet skin-topological effect." We first show the non-Hermitian skin effect can be induced by structured loss when the one-dimensional (1D) system is periodically driven. Next, based on a two-dimensional (2D) Floquet topological photonic lattice with structured loss, we investigate the interaction between the non-Hermiticity and the topological edge states. We observe that all the one-way edge states are imposed onto specific corners, featuring both the non-Hermitian skin effect and topological edge states. Furthermore, a topological switch for the skin-topological effect is presented by utilizing the phase-transition mechanism. Our experiment paves the way for realizing non-Hermitian topological effects in nonlinear and quantum regimes.

Topological insulators are a new phase of matter that is constituted by insulating bulk and conducting edges. They have been extensively explored in condensed matter physics [1,2], photonics [3–11], phononics [12–14], and so on. In photonics, shortly after the observation of topologically protected edge states in microwaves [4], the topological states in the optical frequency range relying on artificial gauge fields were experimentally realized [5,6]. One paradigmatic example is the photonic Floquet topological insulator [5] consisting of a honeycomb array of helical optical waveguides. The periodic driving results in the artificial gauge field and Floquet topological phases. The one-way topological edge states that are immune to backscattering were predicted and observed. The realizations of the topological states in classical-wave systems show potential in lasing [15–18] and quantum sources [19,20].

Characterized by complex eigenenergies and nonorthogonal eigenstates, non-Hermitian physics [21–23] governing systems interacting with the environment has led to many frontiers, such as *PT*-symmetric physics [24–34] and non-Hermitian topological phases [35–45]. Recently, the non-Hermitian skin effect (NHSE) [46–61] has drawn a lot of attention both in theory and experiment. The NHSE features the coalescence of the extended bulk states into the edges of 1D systems, which can be well described by the non-Bloch band theory [52]. The interplay between the NHSE and aforementioned topological states brings us a new concept of the hybrid skin-topological effect [62–67]. Different from the higher-order non-Hermitian skin effect [68–72], the action of the coalescence of extended eigenstates for the skin-topological effect is only on the topological edge modes [63,64]. Therefore, the number of the skin-topological modes is proportional to the length size of the system. To date, such an effect has only been demonstrated by introducing asymmetric coupling into higher-order topolectrical circuits [72], whereas the interaction between the one-way propagating topological edge states and NHSE remains a challenge in experiments.

In this Letter, we bridge this gap by adopting a 2D optical array of lossy helical waveguides and observe the photonic Floquet skin-topological effect. First, by introducing staggered loss into a 1D optical array of helical waveguides, we realize the Floquet non-Hermitian skin effect. Next, we pile up the 1D lattice and arrive at a 2D non-Hermitian Floquet topological insulator. The complex spectrum of the non-Hermitian system shows that the gapless unidirectional edge states spanning across the topological band gap (corresponding to a nonzero Chern number of 1) can acquire the nontrivial point-gap winding topology [63,64,73], which indicates the existence of the NHSE that induced by the nonreciprocal flow of these edge states. In experiments, we observe that all the one-way edge states are imposed onto a specific corner, which reveals the existence of the skin-topological effect that features both the non-Hermitian skin effect and topological edge states. The sign of the winding number determines which corner of the sample is the topological funnel of light. Moreover, by introducing a large enough on-site energy difference and closing the Floquet topological band gap, a topological switch [64,74] for the skin-topological effect is demonstrated.
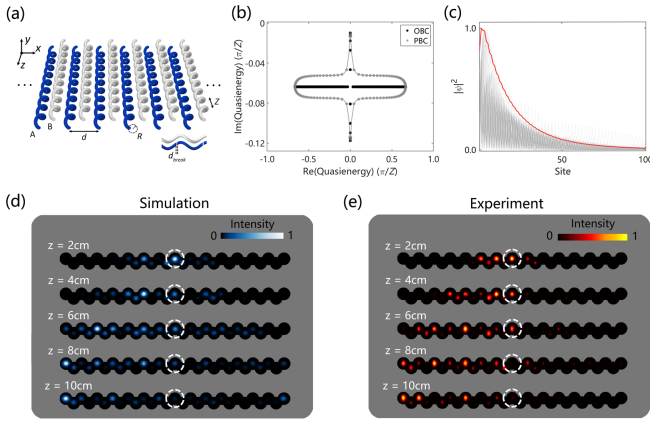
FIG. 1. Floquet NHSE in a 1D optical array. (a) Schematic of a 1D non-Hermitian optical array consisting of helical waveguides. The additional optical loss is introduced into the blue waveguides by setting breakpoints. (b) Complex quasienergy spectrum of the 1D optical array. The spectral loop under PBC indicates the existence of the point-gap topology. (c) Floquet skin eigenmodes (gray curves) and the summing eigenmodes (red curve). The parameters for simulations are coupling strength $c = 1.5$ cm^{-1}, optical loss $\gamma = 0.4$ cm^{-1}, lattice constant $d = 14\sqrt{3}$ μm, helix radius $R = 8$ μm, and the period $Z = 1$ cm. (d),(e) Simulation and experimental results of the Floquet NHSE. The light shifts continuously to the left indicating the collapse of the eigenstates into the left boundary.

We start from a 1D optical array consisting of helical waveguides [shown in Fig. 1(a)]. This 1D optical array contains two sublattices A and B and the sublattice A is endowed with considerable loss, as marked in blue. The paraxial propagation of light in this non-Hermitian system can be described by the tight-binding equation [5]:

$$ i\frac{\partial \psi_n}{\partial z} = \sum_{\langle mn \rangle} c_0 e^{i A(z) \cdot r_{mn}} \psi_m - i\gamma_n \psi_n, \qquad (1) $$

where ψ_n is the electric field amplitude in the nth waveguide, c_0 is the coupling strength between the two nearest waveguides, r_{mn} is the displacement pointing from waveguide m to n, and $\langle mn \rangle$ indicates the summation is taken over nearest-neighboring waveguides. The second term describes the on-site dissipation of the waveguides. The loss at the sublattice A (B) is set to be $\gamma_n = \gamma$ ($\gamma_n = 0$). This z-dependent equation describing paraxial light propagation can be mapped to a time-dependent Schrödinger equation and the z axis plays the role of time. The periodic driving is equivalent to adding a time-dependent vector potential $A(z) = k_0 R\Omega[\sin(\Omega z), -\cos(\Omega z), 0]$ to the optical array, where $k_0 = 2\pi n_0/\lambda$ is the wave number of light in the background medium ($n_0 = 1.45$ is the refractive index of the medium and $\lambda = 635$ nm is the wavelength of light). The distance between the two nearest waveguides is $a = 14$ μm and the lattice constant is $d = 14\sqrt{3}$ μm. The helix radius is $R = 8$ μm and the period is $Z = (2\pi/\Omega) = 1$ cm.

For the above tight-binding model with z-periodic Hamiltonian, its eigenvalues and eigenstates can be calculated from the numerical effective Hamiltonian H_{eff}. The details of the calculations are shown in Supplemental Material [75], Sec. II. The complex quasienergy spectrum of this 1D optical array under periodic boundary condition (PBC) and open boundary condition (OBC) is shown in Fig. 1(b), as labeled by gray dotted curves and black dots, respectively. We can see that the complex spectrum under PBC forms a closed loop and drastically collapses into a line under OBC. The eigenfunctions shown in Fig. 1(c) reveal that the eigenstates all localize at the left boundary, which is the direct result of the NHSE. The closed loop in the complex spectrum results in the nontrivial point-gap topology, which can be characterized by the winding number [46,77] for Floquet systems

$$ w = \int_0^{2\pi} \frac{dk_x}{2\pi i} \partial_{k_x} \log \det[H_{\mathrm{eff}}(k_x) - E_0], \qquad (2) $$

where E_0 is a reference quasienergy for numerical calculations. The winding number for the 1D optical array is $w = 1$ indicating the existence of the NHSE. The result of the generalized Brillouin zone can further verify this point (Supplemental Material, Sec. III [75]).

In experiments, we fabricate the 1D optical array of helical waveguides by utilizing the femtosecond laser writing method [5]. The optical loss in sublattice A is introduced by setting break points periodically into the waveguides [78]. The details of the experiments can be found in Supplemental Material, Sec. VI [75]. To observe the 1D Floquet NHSE, a laser beam with a wavelength of 635 nm is initially launched into the center waveguide of the 1D array. We perform a series of measurements at different propagation lengths of $z = 2$, 4, 6, 8, and 10 cm. The simulation and experimental results are shown in Figs. 1(d) and 1(e). The white dashed circles mark the location of the input waveguide. As we can see, the light propagates continuously to the left, which indicates the collapse of the extended eigenstates onto the left boundary. The experimental results agree well with those from the beam-propagation simulations. This result can also be clearly seen from the dispersion relationship displayed in Supplemental Material, Sec. III [75]. The eigenmodes with low (high) loss have negative (positive) group velocity. Consequently, the left-propagating modes with low loss survive. This observation unravels the existence of 1D NHSE induced by structured loss as well as periodic driving and provides a cornerstone for the next exploration of the interplay between the NHSE and photonic topological edge states.

Having observed the Floquet NHSE in a 1D array, we investigate the interaction between the non-Hermiticity and topological edge states. We pile up the 1D Floquet lattice composed of helical waveguides and arrive at a 2D
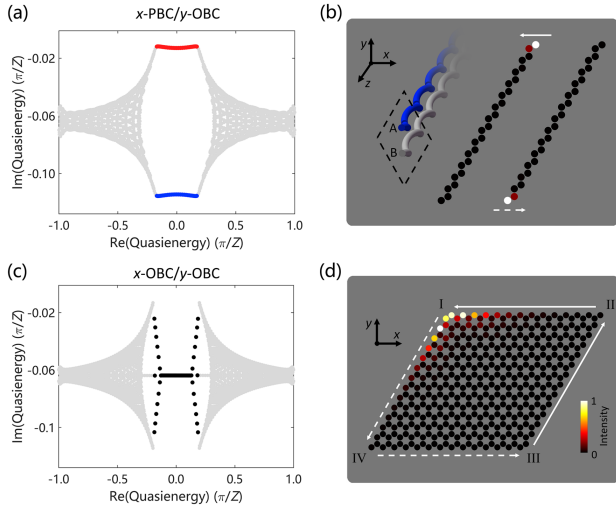
FIG. 2. Hybrid skin-topological effect in a non-Hermitian 2D photonic Floquet topological insulator. (a),(b) Complex quasienergy spectrum under x-PBC/y-OBC. The blue (red) dots correspond to the right (left)-propagating edge mode with relatively larger (negligible) loss. The spectral loop in the topological band gap reveals the nontrivial point-gap topology indicating the existence of the NHSE of light at the boundary. (c), (d), Complex quasienergy spectrum under x-OBC/y-OBC. The skin-topological modes (black dots) emerge and localize at the upper-left corner of the sample (corner I).
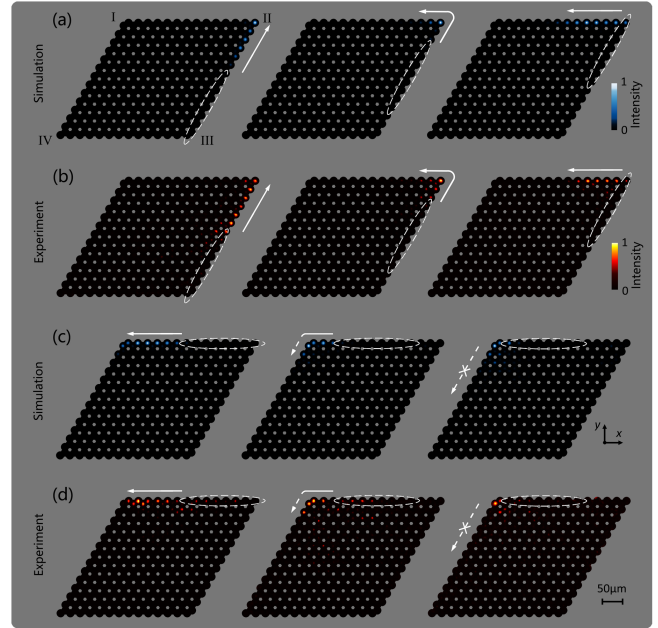

FIG. 3. Simulation (a),(c) and experimental (b),(d) results of the Floquet skin-topological effect. By moving the input tilted Gaussian beam along the outer perimeter, we observe the output light distribution at the end facet of the sample after 10 cm long propagation. (a),(b) The light propagates along the edge of III-II and bypasses the sharp corner II without backscattering. (c),(d), The light propagates along the edge of II-I and accumulates at corner I, which reveals the existence of the Floquet skin-topological corner modes.

photonic non-Hermitian Floquet topological insulator with a nonzero non-Hermitian Chern number [36,73] of $C = 1$ (the detailed calculation is shown in Supplemental Material, Sec. IV [75]). The structured loss is introduced into one sublattice of the honeycomb lattice, as depicted in Fig. 2(b). The nontrivial topology guarantees the existence of the topological boundary states when we consider a finite sample. The complex spectra for two cases of x-PBC/y-OBC (periodic boundary along the x axis and open boundary in the y direction) and x-OBC/y-OBC are shown in Figs. 2(a) and 2(c). Apart from the bulk states marked by gray dotted points, there exist two counter-propagating edge states localized at the opposite edges spanning across the topological band gap in the complex spectrum, as displayed in Figs. 2(a) and 2(b). The blue (red) dots correspond to the right (left)-propagating edge mode with relatively larger (negligible) loss. The complex spectral loop in the topological band gap reveals the nontrivial point-gap topology characterized by the winding number of $w = 1$, which results in the NHSE [46] induced by the one-way edge flow of light. For the case of double OBC (x-OBC/y-OBC), the closed loop in the complex spectrum drastically collapses [Fig. 2(c)] and all non-Hermitian topological edge modes localize at the upper-left corner [labeled as corner I in Fig. 2(d)], whereas the bulk states stay extended (Supplemental Material, Sec. V [75]). The solid (dashed) white arrows pointing to the propagating direction of the edge states correspond to the flow of light

with negligible (larger) loss. As a result, all the energy of the topological edge states accumulates at corner I, which indicates the existence of the so-called hybrid skin-topological modes. Note that if we add the loss configuration on the sublattice B, the point-gap winding will change to $w = -1$, which gives rise to the skin-topological modes at corner III.

To experimentally study the Floquet skin-topological effect, a 2D non-Hermitian honeycomb lattice of helical waveguides is fabricated. The breaks that can generate large optical loss are introduced into the waveguides of sublattice A. To excite the topological edge modes, a broad tilted Gaussian beam is initially launched into the outer perimeter of the sample. The momentum of the Gaussian beam is controlled by a rotated mirror and set to be about $k_x d = \pi$ (Supplemental Material, Sec. VI [75]). The white ellipse indicates the position and shape of the launched Gaussian beam. The total propagation length in the sample is 10 cm (z axis). By moving the injected beam along the outer perimeter, we can see in Figs. 3(a) and 3(b) that the input light can propagate unidirectionally along the edge of III-II, and circumvent the sharp corner II without backscattering. However, the situation changes drastically when the input light encounters corner I, as shown in Figs. 3(c) and 3(d). By moving the input Gaussian beam leftward
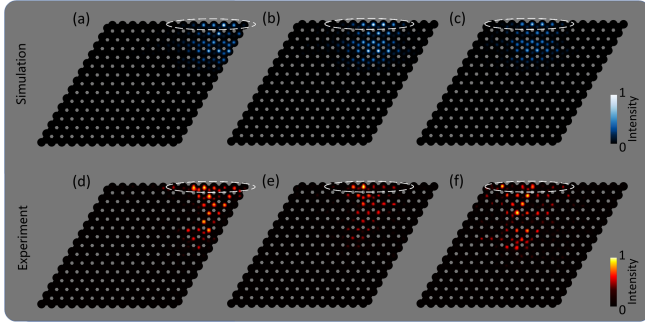
FIG. 4. Topological switch for the skin-topological effect. Introducing a large enough on-site energy difference of $\Delta m = 3.7c_0$ results in the topological phase transition. By moving the input tilted Gaussian beam leftward along the upper edge, we can see that the injected light penetrates into the bulk in both simulations (a)–(c) and experiments (d)–(f). The skin-topological effect is switched off by the phase transition.

along the edge, we observe that the injected light propagates along the upper edge and stays trapped at corner I without penetration into the bulk, which is the direct observation of the hybrid Floquet skin-topological corner modes. The experimental results [Figs. 3(b) and 3(d)] are consistent with the simulation results [Figs. 3(a) and 3(c)]. At this corner I, the ratio of the light energy "accumulated" [Fig. 3(c)] is about 25.6%, which is generally consistent with the value of 30.4% obtained from tight-binding simulations (Supplemental Material, Sec. VII [75]). Note that since the structured loss is introduced in our system, the color bar is rescaled to the maximum in each panel of Fig. 3 for better presentation. The observations in Fig. 3 together elucidate that the Floquet skin-topological effect features both the NHSE and topological protection of the propagating light.

For comparison, we fabricate a 2D Hermitian photonic Floquet topological insulator with no structured loss. We perform the experiments and observe that the initial tilted wave packet can propagate counterclockwise along the outer perimeter and bypasses corner I (Supplemental Material, Sec. IX [75]).

A topological switch [64,74] manifests that topology can provide a switch for the NHSE through topological phase transitions. In our model, by introducing a large on-site energy difference between the two sublattices, the topological phase transition occurs and the Flouqet topological band gap closes. The on-site energy difference of up to $\Delta m \sim 3.7c_0$ can be induced in order to open a trivial band gap through changing the laser-writing speed (see Supplemental Material [75] for more details). Without the topological band gap and topological edge states providing asymmetric coupling for the NHSE, the complex spectrum shows no point-gap winding and therefore no Floquet skin-topological modes can be found. We adopt the same experimental philosophy as shown in Fig. 3. As we can see in Fig. 4, the injected light penetrates into bulk and

cannot accumulate at corner I. Therefore, the skin-topological effect is switched off.

In conclusion, we have experimentally demonstrated the Floquet NHSE in a 1D lossy optical array and Floquet skin-topological effect in a 2D non-Hermitian photonic Floquet topological insulator. By introducing structured loss into the periodically driven optical waveguides, we have found the point-gap topology in the complex spectra of the 1D and 2D non-Hermitian photonic systems. In experiments, we have fabricated the optical lattices by the standard femtosecond laser-writing method and observed the topological funnel of light at the left boundary and corner I of the 1D and 2D optical arrays, respectively. Moreover, a key to switching on and off the skin-topological effect has been realized by utilizing the topological phase transition. Our Letter investigates the interaction between the NHSE and photonic topological edge states and provides the first example of the NHSE in an optical Floquet topological insulator, which may pave the way for further exploration of non-Hermitian topological effects [79,80] in nonlinear [81–83] and quantum regimes [84–86].

*These authors contributed equally to this work.
†zhichao@zju.edu.cn
‡zhaojuyang@zju.edu.cn

[1] M. Z. Hasan and C. L. Kane, Colloquium: Topological insulators, Rev. Mod. Phys. **82,** 3045 (2010).

[2] X.-L. Qi and S.-C. Zhang, Topological insulators and superconductors, Rev. Mod. Phys. **83,** 1057 (2011).

[3] F. D. M. Haldane and S. Raghu, Possible realization of directional optical waveguides in photonic crystals with broken time-reversal symmetry, Phys. Rev. Lett. **100,** 013904 (2008).

[4] Z. Wang, Y. Chong, J. D. Joannopoulos, and M. Soljačić, Observation of unidirectional backscattering-immune topological electromagnetic states, Nature (London) **461,** 772 (2009).

[5] M. C. Rechtsman, J. M. Zeuner, Y. Plotnik, Y. Lumer, D. Podolsky, F. Dreisow, M. Nolte Stefan Segev, and A. Szameit, Photonic Floquet topological insulators, Nature (London) **496,** 196 (2013).

[6] M. Hafezi, S. Mittal, J. Fan, A. Migdall, and J. M. Taylor, Imaging topological edge states in silicon photonics, Nat. Photonics **7,** 1001 (2013).

[7] A. B. Khanikaev, S. H. Mousavi, W.-K. Tse, M. Kargarian, A. H. MacDonald, and G. Shvets, Photonic topological insulators, Nat. Mater. **12,** 233 (2013).

[8] W.-J. Chen, S.-J. Jiang, X.-D. Chen, L. Zhu Baocheng Zhou, J.-W. Dong, and C. T. Chan, Experimental realization of photonic topological insulator in a uniaxial metacrystal waveguide, Nat. Commun. **5,** 5782 (2014).

[9] L.-H. Wu and X. Hu, Scheme for achieving a topological photonic crystal by using dielectric material, Phys. Rev. Lett. **114,** 223901 (2015).

[10] L. Lu, J. D. Joannopoulos, and M. Soljacic, Topological photonics, Nat. Photonics **8,** 821 (2014).

[11] T. Ozawa, H. M. Price, A. Amo, N. Goldman, M. Hafezi, L. Lu, M. C. Rechtsman, D. Schuster, J. Simon, O. Zilberberg, and I. Carusotto, Topological photonics, Rev. Mod. Phys. **91,** 015006 (2019).

[12] S. D. Huber, Topological mechanics, Nat. Phys. **12,** 621 (2016).

[13] G. Ma, M. Xiao, and C. T. Chan, Topological phases in acoustic and mechanical systems, Nat. Rev. Phys. **1,** 281 (2019).

[14] H. Xue, Y. Yang, and B. Zhang, Topological acoustics, Nat. Rev. Mater. **7,** 974 (2022).

[15] B. Bahari, A. Ndao, F. Vallini, A. El Amili, Y. Fainman, and B. Kante, Nonreciprocal lasing in topological cavities of arbitrary geometries, Science **358,** 636 (2017).

[16] M. A. Bandres, S. Wittek, G. Harari, M. Parto, J. Ren, M. Segev, D. N. Christodoulides, and M. Khajavikhan, Topological insulator laser: Experiments, Science **359,** eaar4005 (2018).

[17] Z.-K. Shao, H.-Z. Chen, S. Wang, X.-R. Mao, Z.-Q. Yang, S.-L. Wang, X.-X. Wang, X. Hu, and R.-M. Ma, A high-performance topological bulk laser based on band-inversion-induced reflection, Nat. Nanotechnol. **15,** 67 (2020).

[18] Z. Yang, E. Lustig, G. Harari, Y. Plotnik, Y. Lumer, M. A. Bandres, and M. Segev, Mode-locked topological insulator laser utilizing synthetic dimensions, Phys. Rev. X **10,** 011059 (2020).

[19] S. Mittal, E. A. Goldschmidt, and M. Hafezi, A topological source of quantum light, Nature (London) **561,** 502 (2018).

[20] T. Dai *et al.*, Topologically protected quantum entanglement emitters, Nat. Photonics **16,** 248 (2022).

[21] C. M. Bender and S. Boettcher, Real spectra in non-Hermitian Hamiltonians having $\mathcal{PT}$ symmetry, Phys. Rev. Lett. **80,** 5243 (1998).

[22] Y. Ashida, Z. Gong, and M. Ueda, Non-Hermitian physics, Adv. Phys. **69,** 249 (2020).

[23] E. J. Bergholtz, J. C. Budich, and F. K. Kunst, Exceptional topology of non-Hermitian systems, Rev. Mod. Phys. **93,** 015005 (2021).

[24] A. Guo, G. J. Salamo, D. Duchesne, R. Morandotti, M. Volatier-Ravat, V. Aimez, G. A. Siviloglou, and D. N. Christodoulides, Observation of $\mathcal{PT}$-symmetry breaking in complex optical potentials, Phys. Rev. Lett. **103,** 093902 (2009).

[25] C. E. Rüter, K. G. Makris, R. El-Ganainy, D. N. Christodoulides, M. Segev, and D. Kip, Observation of parity-time symmetry in optics, Nat. Phys. **6,** 192 (2010).

[26] L. Feng, Y. L. Xu, W. S. Fegadolli, M. H. Lu, J. E. B. Oliveira, V. R. Almeida, Y. F. Chen, and A. Scherer, Experimental demonstration of a unidirectional reflectionless parity-time metamaterial at optical frequencies, Nat. Mater. **12,** 108 (2013).

[27] H. Hodaei, M. A. Miri, M. Heinrich, D. N. Christodoulides, and M. Khajavikhan, Parity-time-symmetric microring lasers, Science **346,** 975 (2014).

[28] L. Feng, Z. J. Wong, R. M. Ma, Y. Wang, and X. Zhang, Single-mode laser by parity-time symmetry breaking, Science **346,** 972 (2014).

[29] B. Zhen, C. W. Hsu, Y. Igarashi, L. Lu, I. Kaminer, A. Pick, S.-L. Chua, J. D. Joannopoulos, and M. Soljacic, Spawning rings of exceptional points out of Dirac cones, Nature (London) **525,** 354 (2015).

[30] S. Weimann, M. Kremer, Y. Plotnik, Y. Lumer, K. G. Nolte, S. Makris, M. Segev, M. C. Rechtsman, and A. Szameit, Topologically protected bound states in photonic parity-time-symmetric crystals, Nat. Mater. **16,** 433 (2017).

[31] X. Ni, D. Smirnova, A. Poddubny, D. Leykam, Y. Chong, and A. B. Khanikaev, $\mathcal{PT}$ phase transitions of edge states at $\mathcal{PT}$ symmetric interfaces in-Hermitian topological insulators, Phys. Rev. B **98,** 165129 (2018).

[32] R. El-Ganainy, K. G. Makris, Z. H. Khajavikhan Mercedeh Musslimani, S. Rotter, and D. N. Christodoulides, Non-Hermitian physics and PT symmetry, Nat. Phys. **14,** 11 (2018).

[33] K. Özdemir, S. Rotter, F. Nori, and L. Yang, Parity-time symmetry and exceptional points in photonics, Nat. Mater. **18,** 783 (2019).

[34] M. A. Miri and A. Alù, Exceptional points in optics and photonics, Science **363,** eaar7709 (2019).

[35] J. M. Zeuner, M. C. Rechtsman, Y. Plotnik, Y. Lumer, S. Nolte, M. S. Rudner, M. Segev, and A. Szameit, Observation of a topological transition in the bulk of a non-Hermitian system, Phys. Rev. Lett. **115,** 040402 (2015).

[36] S. Yao, F. Song, and Z. Wang, Non-Hermitian Chern bands, Phys. Rev. Lett. **121,** 136802 (2018).

[37] K. Kawabata, K. Shiozaki, M. Ueda, and M. Sato, Symmetry and topology in non-Hermitian physics, Phys. Rev. X **9,** 041015 (2019).

[38] T. Liu, Y.-R. Zhang, Q. Ai, Z. Gong, K. Kawabata, M. Ueda, and F. Nori, Second-order topological phases in non-Hermitian systems, Phys. Rev. Lett. **122,** 076801 (2019).

[39] X.-W. Luo and C. Zhang, Higher-order topological corner states induced by gain and loss, Phys. Rev. Lett. **123,** 073601 (2019).

[40] Z. Zhang, M. Rosendo Lopez, Y. Cheng, X.-J. Liu, and J. Christensen, Non-Hermitian sonic second-order topological insulator, Phys. Rev. Lett. **122,** 195501 (2019).

[41] H. Zhao, X. Qiao, T. Wu, B. Midya, S. Longhi, and L. Feng, Non-Hermitian topological light steering, Science **365,** 1163 (2019).

[42] F. E. Öztürk, T. Lappe, G. Hellmann, J. Schmitt, J. Klaers, F. Vewinger, J. Kroha, and M. Weitz, Observation of a non-Hermitian phase transition in an optical quantum gas, Science **372,** 88 (2021).

[43] B. Hu *et al.*, Non-Hermitian topological whispering gallery, Nature (London) **597,** 655 (2021).

[44] K. Wang, A. Dutt, K. Y. Yang, C. C. Wojcik, J. Vučković, and S. Fan, Generating arbitrary topological windings of a non-Hermitian band, Science **371,** 1240 (2021).

[45] K. Wang, A. Dutt, C. C. Wojcik, and S. Fan, Topological complex-energy braiding of non-Hermitian bands, Nature (London) **598,** 59 (2021).

[46] S. Yao and Z. Wang, Edge states and topological invariants of non-Hermitian systems, Phys. Rev. Lett. **121,** 086803 (2018).

[47] F. Song, S. Yao, and Z. Wang, Non-Hermitian skin effect and chiral damping in open quantum systems, Phys. Rev. Lett. **123**, 170401 (2019).

[48] F. Song, S. Yao, and Z. Wang, Non-Hermitian topological invariants in real space, Phys. Rev. Lett. **123**, 246801 (2019).

[49] K. Yokomizo and S. Murakami, Non-Bloch band theory of non-Hermitian systems, Phys. Rev. Lett. **123**, 066404 (2019).

[50] Y. Yi and Z. Yang, Non-Hermitian skin modes induced by on-site dissipations and chiral effect, Phys. Rev. Lett. **125**, 186802 (2020).

[51] K. Zhang, Z. Yang, and C. Fang, Correspondence between winding numbers and skin modes in non-Hermitian, Phys. Rev. Lett. **125**, 126402 (2020).

[52] Z. Yang, K. Zhang, C. Fang, and J. Hu, Non-Hermitian bulk-boundary correspondence and auxiliary generalized zone theory, Phys. Rev. Lett. **125**, 226402 (2020).

[53] S. Weidemann, M. Kremer, T. Helbig, T. Hofmann, A. Stegmaier, M. Greiter, R. Thomale, and A. Szameit, Topological funneling of light, Science **368**, 311 (2020).

[54] L. Xiao, T. Deng, K. Wang, G. Zhu, Z. Wang, W. Yi, and P. Xue, Non-Hermitian bulk-boundary correspondence in quantum dynamics, Nat. Phys. **16**, 761 (2020).

[55] N. Okuma, K. Kawabata, K. Shiozaki, and M. Sato, Topological origin of non-Hermitian skin effects, Phys. Rev. Lett. **124**, 086801 (2020).

[56] T. Helbig, T. Hofmann, S. Imhof, M. Abdelghany, T. Kiessling, L. W. Molenkamp, C. H. Lee, A. Szameit, M. Greiter, and R. Thomale, Generalized bulk-boundary correspondence in non-Hermitian topolectrical circuits, Nat. Phys. **16**, 747 (2020).

[57] H. Wu and J. H. An, Floquet topological phases of non-Hermitian systems, Phys. Rev. B **102**, 041119(R) (2020).

[58] Q. Liang, D. Xie, Z. Dong, H. Li, H. Li, B. Gadway, W. Yi, and B. Yan, Dynamic signatures of non-Hermitian skin effect and topology in ultracold atoms, Phys. Rev. Lett. **129**, 070401 (2022).

[59] H. Gao, H. Xue, Z. Gu, L. Li, W. Zhu, Z. Su, J. Zhu, B. Zhang, and Y. D. Chong, Anomalous Floquet non-Hermitian skin effect in a ring resonator lattice, Phys. Rev. B **106**, 134112 (2022).

[60] Z. Gu, H. Gao, H. Xue, J. Li, Z. Su, and J. Zhu, Transient non-Hermitian skin effect, Nat. Commun. **13**, 7668 (2022).

[61] S. Ke, W. Wen, D. Zhao, and Y. Wang, Floquet engineering of the non-Hermitian skin effect in photonic waveguide arrays, Phys. Rev. A **107**, 053508 (2023).

[62] C. H. Lee, L. Li, and J. Gong, Hybrid higher-order skin-topological modes in nonreciprocal systems, Phys. Rev. Lett. **123**, 016805 (2019).

[63] Y. Li, C. Liang, C. Wang, C. Lu, and Y.-C. Liu, Gain-loss-induced hybrid skin-topological effect, Phys. Rev. Lett. **128**, 223903 (2022).

[64] W. Zhu and J. Gong, Hybrid skin-topological modes without asymmetric couplings, Phys. Rev. B **106**, 035425 (2022).

[65] H. Liu and I. Fulga, Mixed higher-order topology: Boundary non-Hermitian skin effect induced by a Floquet bulk, Phys. Rev. B **108**, 035107 (2023).

[66] W. Zhu and J. Gong, Photonic corner skin modes in non-Hermitian photonic crystals, Phys. Rev. B **108**, 035406 (2023).

[67] Y. Li, C. Lu, S. Zhang, and Y. Liu, Loss-induced Floquet non-Hermitian skin effect, Phys. Rev. B **108**, L220301 (2023).

[68] K. Kawabata, M. Sato, and K. Shiozaki, Higher-order non-Hermitian skin effect, Phys. Rev. B **102**, 205118 (2020).

[69] R. Okugawa, R. Takahashi, and K. Yokomizo, Second-order topological non-Hermitian skin effects, Phys. Rev. B **102**, 241202(R) (2020).

[70] Y. Fu, J. Hu, and S. Wan, Non-Hermitian second-order skin and topological modes, Phys. Rev. B **103**, 045420 (2021).

[71] X. Zhang, Y. Tian, J.-H. Jiang, M.-H. Lu, and Y.-F. Chen, Observation of higher-order non-Hermitian skin effect, Nat. Commun. **12**, 5377 (2021).

[72] D. Zou, T. Chen, W. He, J. Bao, C. H. Lee, H. Sun, and X. Zhang, Observation of hybrid higher-order skin-topological effect in non-Hermitian topolectrical circuits, Nat. Commun. **12**, 7201 (2021).

[73] H. Shen, B. Zhen, and L. Fu, Topological band theory for non-Hermitian Hamiltonians, Phys. Rev. Lett. **120**, 146402 (2018).

[74] L. Li, C. H. Lee, and J. Gong, Topological Switch for non-Hermitian skin effect in cold-atom systems with loss, Phys. Rev. Lett. **124**, 250402 (2020).

[75] See Supplemental Material at http://link.aps.org/supplemental/10.1103/PhysRevLett.132.063804 for details, which includes Ref. [76].

[76] G. Jotzu, M. Messer, R. Desbuquois, M. Lebrat, T. Uehlinger, D. Greif, and T. Esslinger, Experimental realization of the topological Haldane model with ultracold fermions, Nature (London) **515**, 237 (2014).

[77] Z. Gong, Y. Ashida, K. Kawabata, K. Takasan, S. Higashikawa, and M. Ueda, Topological phases of non-Hermitian systems, Phys. Rev. X **8**, 031079 (2018).

[78] A. Cerjan, S. Huang, M. Wang, K. P. Chen, Y. Chong, and M. C. Rechtsman, Experimental realization of a Weyl exceptional ring, Nat. Photonics **13**, 623 (2019).

[79] K. Zhang, Z. Yang, and C. Fang, Universal non-Hermitian skin effect in two and higher dimensions, Nat. Commun. **13**, 2496 (2022).

[80] T. Wan, K. Zhang, J. Li, Z. Yang, and Z. Yang, Observation of dynamical degeneracy splitting for the non-Hermitian skin effect, Sci. Bull. **68**, 2330 (2023).

[81] L. J. Maczewsky *et al.*, Nonlinearity-induced photonic topological insulator, Science **370**, 701 (2020).

[82] S. Mukherjee and M. C. Rechtsman, Observation of Floquet solitons in a topological bandgap, Science **368**, 856 (2020).

[83] S. Xia, D. Kaltsas, D. Song, I. Komis, J. Xu, A. Szameit, H. Buljan, K. G. Makris, and Z. Chen, Nonlinear tuning of PT symmetry and non-Hermitian topological states, Science **372**, 72 (2021).

[84] S. Barik, A. Karasahin, C. Flower, T. Cai, H. Miyake, W. DeGottardi, M. Hafezi, and E. Waks, A topological quantum optics interface, Science **359**, 666 (2018).

[85] J. Deng *et al.*, Observing the quantum topology of light, Science **378**, 966 (2022).

[86] Z. Dong, H. Li, T. Wan, Q. Liang, Z. Yang, and B. Yan, Quantum time reflection and refraction of ultracold atoms, Nat. Photonics **18**, 68 (2023).